Cell Reports

SIRT6 Suppresses Cancer Stem-like Capacity in Tumors with PI3K Activation Independently of Its Deacetylase Activity

Graphical Abstract

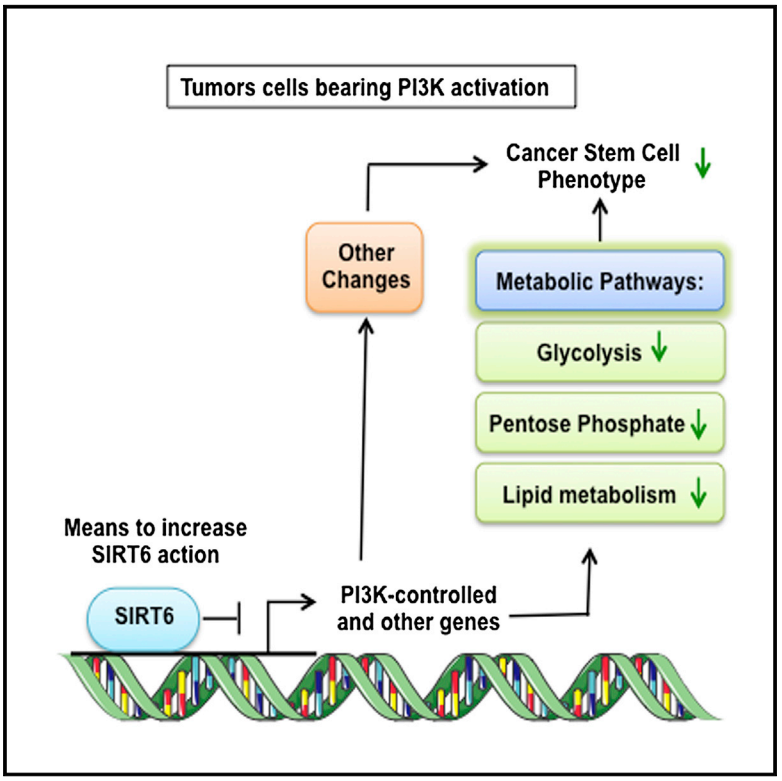

Highlights

- Enhanced SIRT6 hinders stemness of human cancer cells with PI3K activation
- Enhanced SIRT6 rearranges metabolism of cancer cells with PI3K activation
- Enhanced SIRT6 reduces grade and progression of murine tumors with PI3K activation
- Anti-cancer-stemness action is independent of SIRT6 histone deacetylase activity

Authors

Rafael M. Ioris, Mirco Galié, Giorgio Ramadori, ..., Raul Mostoslavsky, Pierre Baldi, Roberto Coppari

Correspondence

roberto.coppari@unige.ch

In Brief

Ioris et al. provide in vitro and in vivo evidence that enhanced SIRT6 suppresses cancer progression and stemness in the context of constitutively active PI3K signaling. This effect is, at least in part, through suppression of the PI3K pathway at the transcriptional level and independent of SIRT6's histone deacetylase activity.

Accession Numbers

GSE93837

source: https://doi.org/10.7892/boris.96842 | downloaded: 5.5.2023

Ioris et al., 2017, Cell Reports *18*, 1858–1868
February 21, 2017 © 2017 The Author(s).
http://dx.doi.org/10.1016/j.celrep.2017.01.065

CellPress

OPEN ACCESS
CellPress

Cell Reports
Report

SIRT6 Suppresses Cancer Stem-like Capacity in Tumors with PI3K Activation Independently of Its Deacetylase Activity

Rafael M. Ioris,[1,2,11] Mirco Galié,[1,3,11] Giorgio Ramadori,[1,2,11] Jason G. Anderson,[4] Anne Charollais,[1,2] Georgia Konstantinidou,[5] Xavier Brenachot,[1,2] Ebru Aras,[1,2] Algera Goga,[1,2] Nicholas Ceglia,[6,7] Carlos Sebastián,[8,9] Denis Martinvalet,[1] Raul Mostoslavsky,[8,9,10] Pierre Baldi,[6,7] and Roberto Coppari[1,2,12,*]

[1]Department of Cell Physiology and Metabolism, Faculty of Medicine, University of Geneva, 1211 Geneva 4, Switzerland
[2]Diabetes Center of the Faculty of Medicine, University of Geneva, 1211 Geneva 4, Switzerland
[3]Department of Neurosciences, Biomedicine and Movement, University of Verona, Verona 37134, Italy
[4]Department of Internal Medicine, Division of Hypothalamic Research, The University of Texas Southwestern Medical Center, Dallas, TX 75390, USA
[5]Institute of Pharmacology, University of Bern, 3010 Bern, Switzerland
[6]Department of Computer Science University of California Irvine, Irvine, CA 92697, USA
[7]Institute for Genomics and Bioinformatics, University of California Irvine, Irvine, CA 92697, USA
[8]The Massachusetts General Hospital Cancer Center, Harvard Medical School, Boston, MA 02114, USA
[9]The MGH Center for Regenerative Medicine, Harvard Medical School, Boston, MA 02114, USA
[10]The Broad Institute of Harvard and MIT, Cambridge, MA 02142, USA
[11]Co-first author
[12]Lead Contact
*Correspondence: roberto.coppari@unige.ch
http://dx.doi.org/10.1016/j.celrep.2017.01.065

SUMMARY

Cancer stem cells (CSCs) have high tumorigenic capacity. Here, we show that stem-like traits of specific human cancer cells are reduced by overexpression of the histone deacetylase sirtuin 6 (SIRT6). SIRT6-sensitive cancer cells bear mutations that activate phosphatidylinositol-3-kinase (PI3K) signaling, and overexpression of SIRT6 reduces growth, progression, and grade of breast cancer in a mouse model with PI3K activation. Tumor metabolomic and transcriptomic analyses reveal that SIRT6 overexpression dampens PI3K signaling and stem-like characteristics and causes metabolic rearrangements in this cancer model. Ablation of a PI3K activating mutation in otherwise isogenic cancer cells is sufficient to convert SIRT6-sensitive into SIRT6-insensitive cells. SIRT6 overexpression suppresses PI3K signaling at the transcriptional level and antagonizes tumor sphere formation independent of its histone deacetylase activity. Our data identify SIRT6 as a putative molecular target that hinders stemness of tumors with PI3K activation.

INTRODUCTION

Cancer kills approximately 8 million people annually (World Health Organization fact sheet number 297). Although anti-cancer therapy is rapidly improving, further therapeutic development is urgently needed. The idea that subpopulations of cells within the tumor mass, cancer stem cells (CSCs) (or tumor-initiating cells), have high tumorigenic and self-renewal ability was proposed more than 20 years ago (Lapidot et al., 1994; Pattabiraman and Weinberg, 2014; Wang and Dick, 2005). Since then, CSCs have been identified in several human tumors (e.g., leukemia, breast, brain, prostate, colon, and pancreatic cancers), and the notion of eradicating cancer by eroding the CSC pool has started to show potential in humans (Lapidot et al., 1994; Pattabiraman and Weinberg, 2014; Prost et al., 2015). Despite the fact that significant efforts aimed at identifying molecular targets to hinder cancer stemness have been made, these anti-CSCs targets remain poorly understood.

The roles of epigenetic changes (e.g., histone modifications) on cancer behavior and stemness are appreciated. For example, it has recently been shown that protein kinase A indirectly affects histone methylation and expression of epithelial genes, an effect that hinders CSC activity and promotes tumor differentiation, a feature associated with better prognosis (Pattabiraman et al., 2016). The histone deacetylase SIRT6 has been suggested to affect tumor behavior as (1) *Sirt6* loss of function facilitates progression of cancer in mice (Kugel et al., 2016; Sebastián et al., 2012), (2) *Sirt6* loss-of-function mutations have been found in human cancers (Kugel et al., 2015), and (3) SIRT6 expression in tumor lesions positively correlates with survival of cancer patients (Sebastián et al., 2012; Thirumurthi et al., 2014). Although these loss-of-function results suggest that SIRT6 is a tumor suppressor, others have shown opposite outcomes (Ming et al., 2014). Whether enhanced SIRT6 function obstructs tumor progression and/or CSCs is unclear.

In this study, we assessed the outcomes of enhanced SIRT6 action in different human and murine cancers. Surprisingly, we found that mutations leading to PI3K activation predict

 © 2017 The Author(s).
This is an open access article under the CC BY-NC-ND license (http://creativecommons.org/licenses/by-nc-nd/4.0/).

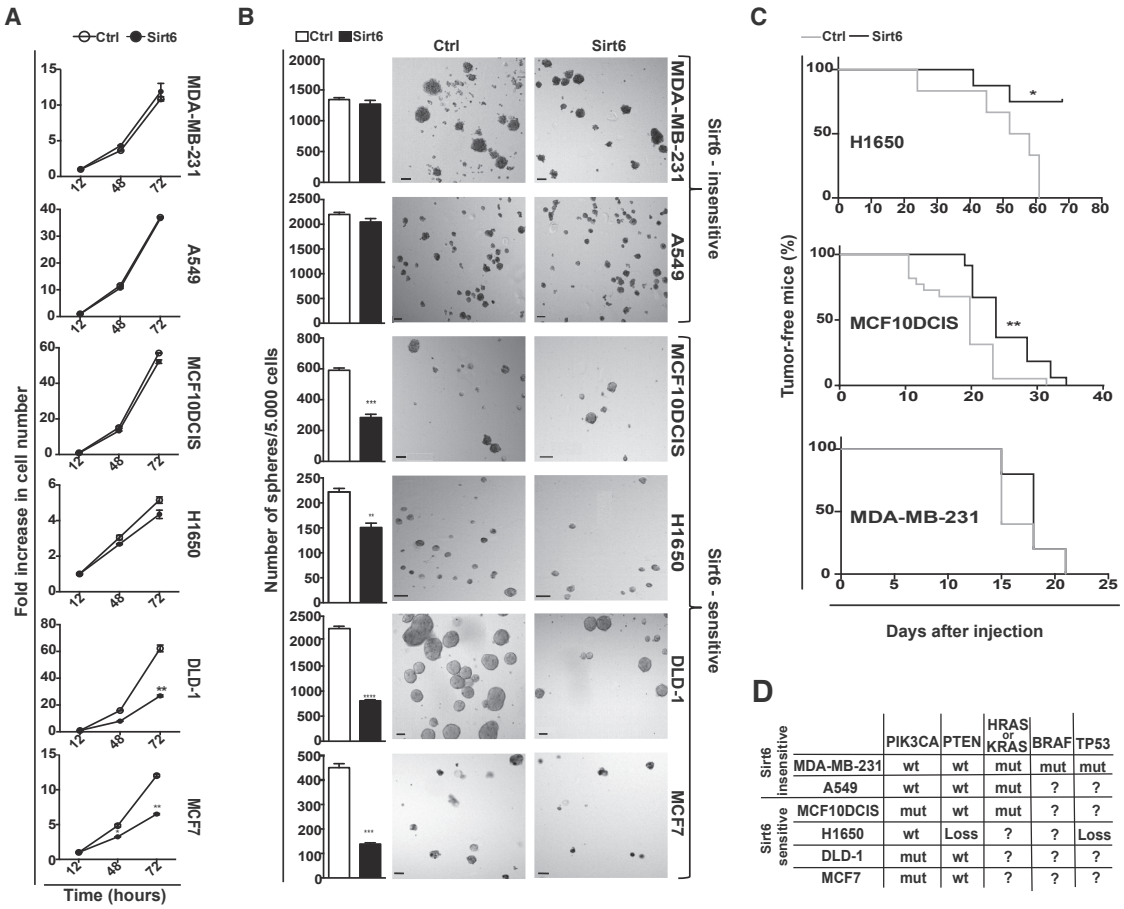

		PIK3CA	PTEN	HRAS or KRAS	BRAF	TP53
Sirt6 insensitive	MDA-MB-231	wt	wt	mut	mut	mut
	A549	wt	wt	mut	?	?
Sirt6 sensitive	MCF10DCIS	mut	wt	mut	?	?
	H1650	wt	Loss	?	?	Loss
	DLD-1	mut	wt	?	?	?
	MCF7	mut	wt	?	?	?

Figure 1. SIRT6 Thwarts Stemness and Tumorigenic Capacity of Human Cancer Cells with PI3K Activation

(A and B) Proliferation (A) and tumorsphere-forming capacity (B) of indicated cells harboring empty vector (Ctrl) or a vector overexpressing human SIRT6 (Sirt6).

(C) Kaplan-Meier curves comparing percentage of tumor-free mice at different times after subcutaneous injection of indicated cells harboring empty vector (Ctrl) or a vector overexpressing human SIRT6 (Sirt6).

(D) Known mutational status of indicated cancer cells.

In (A) and (B), *p < 0.05, **p < 0.01, ***p < 0.001 (two-tailed unpaired Student's t test). Error bars represent SEM. In (C), *p < 0.05, **p < 0.01 (long-rank test). See also Figure S1.

responsiveness to the anti-cancer-stemness action of SIRT6 overexpression.

RESULTS

Differential Responsiveness of Human Cancer Cells to Enhanced SIRT6 Action

To determine the effect of enhanced SIRT6 expression on tumor biology, six different cancer cells obtained from breast (MDA-MB-231, MCF7, and MCF10DCIS), lung (H1650 and A549), and colorectal (DLD-1) human tumors were transduced with either a control vector or a vector expressing SIRT6. As expected, the latter showed increased SIRT6 protein content compared to controls (Figure S1A). Surprisingly only DLD-1 and MCF7 cells displayed reduced proliferation upon SIRT6 overexpression (Figure 1A). Because SIRT6 overexpression has been shown to cause apoptosis in cancer cells (including MDA-MB-231 cells) (Van Meter et al., 2011), we investigated whether changes in apoptosis could underlie the anti-proliferative action of SIRT6 overexpression. Although enhanced SIRT6 expression caused variegate effects on the cell-cycle phases, it was not accompanied by induction of apoptosis because (1) the percentage of the $SubG_0$ population and (2) the level of apoptosis markers cleaved caspase 3 and PARP1 were not significantly different between cells overexpressing SIRT6 and their controls (Figures S1B and S1C). We suggest that the discrepancy between our results and the ones reported by Van Meter and colleagues is due to the different approaches (transient transfection [Van Meter et al., 2011] versus stable transfection [this study]) used to induce SIRT6 overexpression.

When the ability to form tumorsphere in three-dimensional cultures, which is an established readout of CSCs (Dontu et al., 2003; Ponti et al., 2005; Rasheed et al., 2010), was assessed, we found that SIRT6 overexpression drastically decreases tumorsphere-forming capacity of MCF10DCIS, MCF7, H1650,

and DLD-1 cells, while it causes no changes in MDA-MB-231 or A549 cells (Figure 1B). To independently assess cancer stemness, the size of the cell population with high aldehyde dehydrogenase (ALDH) activity was measured (Carpentino et al., 2009; Cheung et al., 2007; Ginestier et al., 2007). This parameter was found to be reduced in H1650 and MCF10DCIS cells (Figure S1D). To directly test whether cancer cells with high ALDH activity ($ALDH^{high}$) represented in Figure S1D are enriched in CSCs, we compared their tumorsphere-forming capacity with the one of cells with low ALDH activity ($ALDH^{low}$). In agreement with previous reports (Ginestier et al., 2007; Liu et al., 2011; Yang et al., 2010), $ALDH^{high}$ cells gave rise to a higher number of tumorspheres compared to $ALDH^{low}$ cells (Figure S1E), hence supporting that $ALDH^{high}$ cells are enriched in CSCs. Collectively, our data indicate that cancer cells could be categorized into two groups: SIRT6-sensitive cells, which show significant reduction in their stem-like trait (MCF10DCIS, MCF7, H1650, and DLD-1) and SIRT6-insensitive cells (MDA-MB-231 and A549) whose stem-like trait is unaffected by SIRT6 overexpression.

Reduced number of CSCs should lead to reduced tumorigenic capacity in vivo. To test this possibility, SIRT6-sensitive (H1650 and MCF10DCIS) and SIRT6-insensitive (MDA-MB-231) cells were injected into the flank of non-obese diabetic/severe combined immunodeficient (NOD/SCID) mice and their growth was monitored over time. Results shown in Figure 1C demonstrate that while SIRT6 overexpression does not affect appearance of SIRT6-insensitive MDA-MB-231 xenografts it significantly delays this parameter of SIRT6-sensitive H1650 and MCF10DCIS xenografts. Hence, our data suggest that enhanced SIRT6 expression hinders stemness and tumorigenic capacity of specific human cancer cells.

By surveying the mutations characterizing SIRT6-sensitive and -insensitive cells, we found that SIRT6-sensitive cells bear mutations in genes regulating PI3K signaling while SIRT6-insensitive cells do not. Specifically, MCF10DCIS and MCF7 and DLD-1 cells bear an activating mutation (H1047R and E545K, respectively) in *PIK3CA* gene (Kalaany and Sabatini, 2009; Samuels et al., 2005; Su et al., 2015). Also, H1650 cells are characterized by *PTEN* (phosphate and tensin homolog deleted on chromosome 10) loss (Sos et al., 2009) (Figure 1D). On the other hand, MDA-MB-231 and A549 cells are not known to have PI3K activating mutations (Kalaany and Sabatini, 2009; Ramadori et al., 2015) (Figure 1D). In keeping with their genetic types, phosphorylation status of serine 473 of AKT (P-S473-AKT), which is an established marker of PI3K signaling, was enhanced in SIRT6-sensitive cells; yet, SIRT6 overexpression did not affect, or only marginally affected (e.g., DLD-1 cells), AKT phosphorylation suggesting that it does not influence PI3K signaling at the AKT level (Figure S1A). In summary, our data indicate that the anti-tumor action of SIRT6 overexpression is favored in the context of PI3K activation.

Enhanced SIRT6 Hinders Progression of Breast Cancer with PI3K Activation in Mice

Suppression of the CSCs pool is predicted to hinder progression toward high-grade lesions and promote tumor differentiation, a characteristic associated with better prognosis (Pattabiraman et al., 2016). The transgenic mouse expressing polyomavirus middle T oncogene (PyMT) under the mouse mammary tumor virus promoter is an established animal model mimicking progression of human breast cancers originating from hyperplastic lesions to high-grade carcinomas; also, these tumors display PI3K activation (Guy et al., 1992; Lin et al., 2003) (Figures S2A and S2B). Thus, to assess whether enhanced SIRT6 affects stemness and progression of a breast tumor with PI3K activation we crossed genetically engineered mice overexpressing functionally competent SIRT6 protein (Sirt6BAC mice) (Anderson et al., 2015) to PyMT mice. Tumor lesions of mice carrying both PyMT and Sirt6BAC alleles (PyMT/Sirt6 mice) were assessed for SIRT6 expression. Data shown in Figures 2A and 2B indicate that tumors from PyMT/Sirt6 mice have enhanced SIRT6 expression compared to their controls bearing only the PyMT allele. Of note, Sirt6BAC allele had no effect on expression of the oncogene driving tumorigenesis in this cancer model as PyMT mRNA level is similar between groups (Figure 2C). Due to its histone deacetylase activity, SIRT6 overexpression is expected to dampen expression of its target genes. Indeed, gene set enrichment analysis (Subramanian et al., 2005) of whole-genome microarray data showed that mRNA levels of several SIRT6's target genes (Kawahara et al., 2011) are reduced in tumors of PyMT/Sirt6 mice compared to controls (Figure 2D). Noteworthy, a number of mRNA changes identified by microarray assay were confirmed by real-time qPCR analysis (Figures S2C and S2D). Collectively, these results demonstrate that the Sirt6BAC allele brings about enhanced SIRT6 expression and activity in PyMT-driven breast tumors in mice.

To test the consequence of increased SIRT6 function on this cancer model, we analyzed several tumor parameters. PyMT/Sirt6 mice displayed a delay in tumor appearance (Figure S2E). At 12 weeks of age, tumor volume, weight, and number were all found to be reduced in PyMT/Sirt6 compared to controls (Figure 2E). Tumor growth rate, assessed by tumor diameter evolution after its detection, was also found to be significantly reduced in PyMT/Sirt6 mice (Figure 2F). To better understand this anti-tumor action of SIRT6 overexpression, we performed histological analyses. In keeping with our in vitro results shown in Figures S1B and S1C, TUNEL assay indicated that altered apoptotic rate is unlikely to be involved because the portion of TUNEL-positive cells in tumor samples was similar between groups (Figure S2F). Notably, while the percentage of necrotic, hyperplastic, or adenomatous-like area (low-grade tumor) was unchanged, the carcinomatous area, which represents the more aggressive/high-grade tumor lesion, was reduced nearly by a factor of two in tumors of PyMT/Sirt6 mice compared to controls (Figure 2G). These results indicate that enhanced SIRT6 expression/activity keeps this breast cancer model more differentiated, a characteristic associated with better prognosis (Pattabiraman et al., 2016). In line with this notion, several genes typically expressed by differentiated mammary gland epithelia were found to be overexpressed in tumors of PyMT/Sirt6 mice compared to controls (Figures 2H and S2G). Together, our data demonstrate that enhanced SIRT6 function inhibits growth and promotes differentiation of a breast cancer model with PI3K activation.

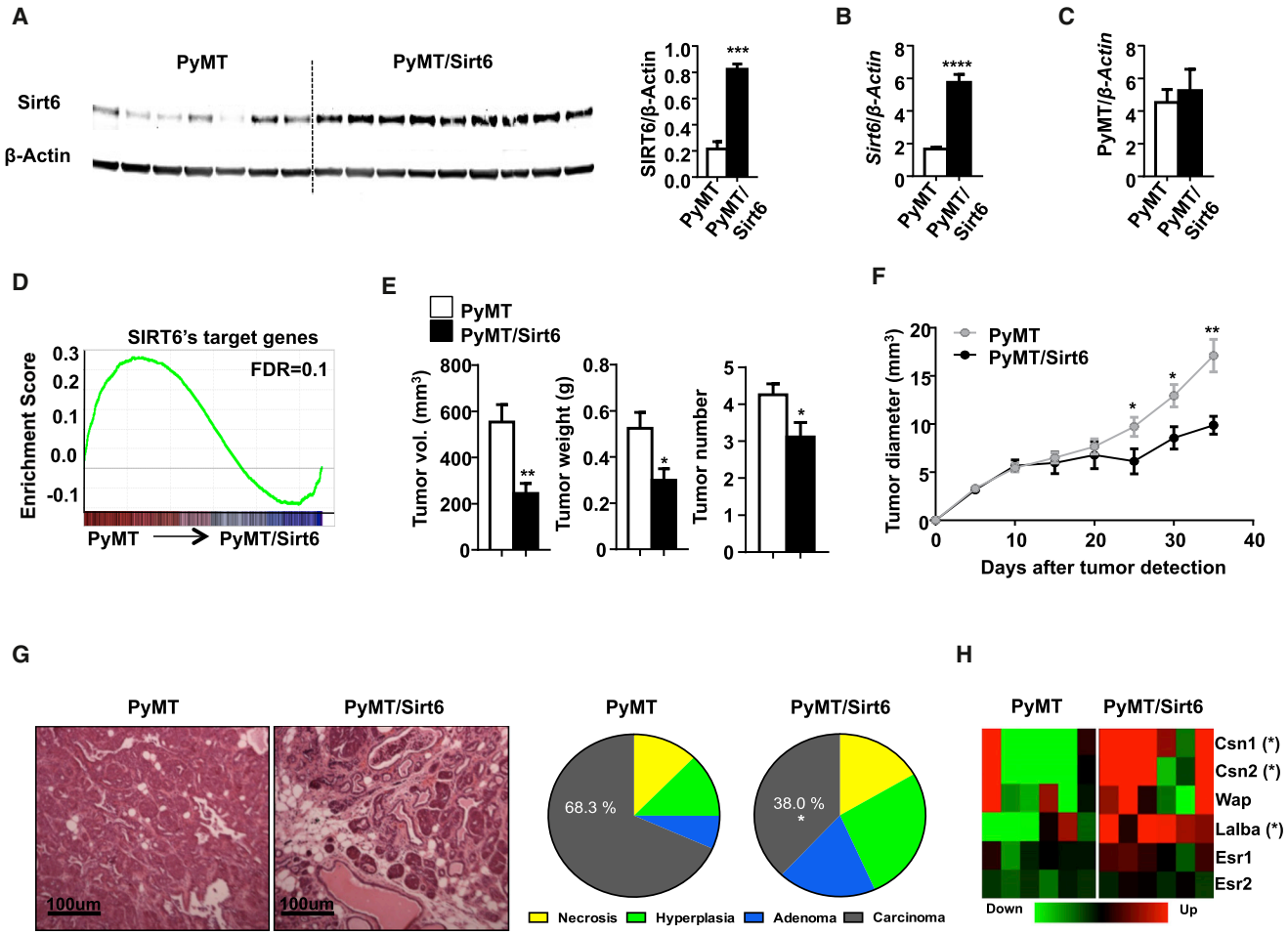

Figure 2. SIRT6 Overexpression Hinders Progression of PyMT-Driven Breast Cancer in Mice

(A) Immunoblot image and quantification of SIRT6 level normalized to β-Actin content in tumors of 12- to 14-week-old PyMT and PyMT/Sirt6 mice.

(B and C) mRNA levels of *Sirt6* (B) and of PyMT (C) normalized to *β-Actin* mRNA content in tumors of 12- to 14-week-old PyMT (n = 7) and PyMT/Sirt6 (n = 8) mice.

(D) Gene set enrichment analysis (GSEA) plot showing the enrichment score (ES) of SIRT6's target genes as indicated in table S2 of Kawahara and colleagues (Kawahara et al., 2011). Gene microarray was performed using RNA extracted from tumors of 12- to 14-week-old PyMT (n = 6) and PyMT/Sirt6 (n = 6) mice.

(E) Tumor volume, weight, and number per mouse in 12-week-old PyMT (n = 18) and PyMT/Sirt6 (n = 18) mice.

(F) Diameter evolution over time of tumors in PyMT and PyMT/Sirt6 mice.

(G) Representative images of tumors stained with H&E (scale bar, 100 μm) and percentage of area of necrosis, adenoma, hyperplasia, and carcinoma in similar-size tumors from PyMT and PyMT/Sirt6 mice (n = 9–10 per group). Scoring of necrosis, adenoma, hyperplasia, and carcinoma was performed on whole tumor area of H&E-stained tissues.

(H) Expression profile of normal mammary epithelial markers using microarray data as in (D).

In (A)–(H), *p < 0.05, **p < 0.01, ***p < 0.001, ****p < 0.0001 (two-tailed unpaired Student's t test). Error bars represent SEM. In (D), FDR, false discovery rate q value. See also Figure S2.

Enhanced SIRT6 Rearranges Metabolism and Suppresses PI3K Signaling and Stem-like Traits in Breast Tumors

To understand the mechanisms underlying the anti-tumor action of SIRT6 overexpression, we performed metabolomic and transcriptomic analyses. By comparing our transcriptomic data with 246 publicly available microarray datasets including embryonic stem cells (ESCs), adult stem cells (ASCs), induced pluripotent stem (iPS) cells, and terminally differentiated tissues (TDTs) (Barger et al., 2008; Mikkelsen et al., 2007, 2008; Sampath et al., 2008; Seale et al., 2007; Thorrez et al., 2008; Ulloa-Montoya et al., 2007), we found that genes downregulated in tumors of PyMT/Sirt6 mice (Figure S3A; Table S1) are enriched in stem cells (ESC, iPS cells, and ASCs) (Figure 3A). Also, we analyzed the enrichment of genes on microarray datasets of human breast cancers (van de Vijver et al., 2002). These samples were classified in normal-like, basal-like, HER2, Claudin-low, and luminal subtypes according to previous reports (Sorlie et al., 2003). Our results indicated that the genes downregulated in tumors of PyMT/Sirt6 mice are enriched in basal-like/Claudin-low tumors (Figure 3B), which represent the most stem-like/aggressive breast cancer types (Ben-Porath et al., 2008; Sorlie et al., 2003). To independently

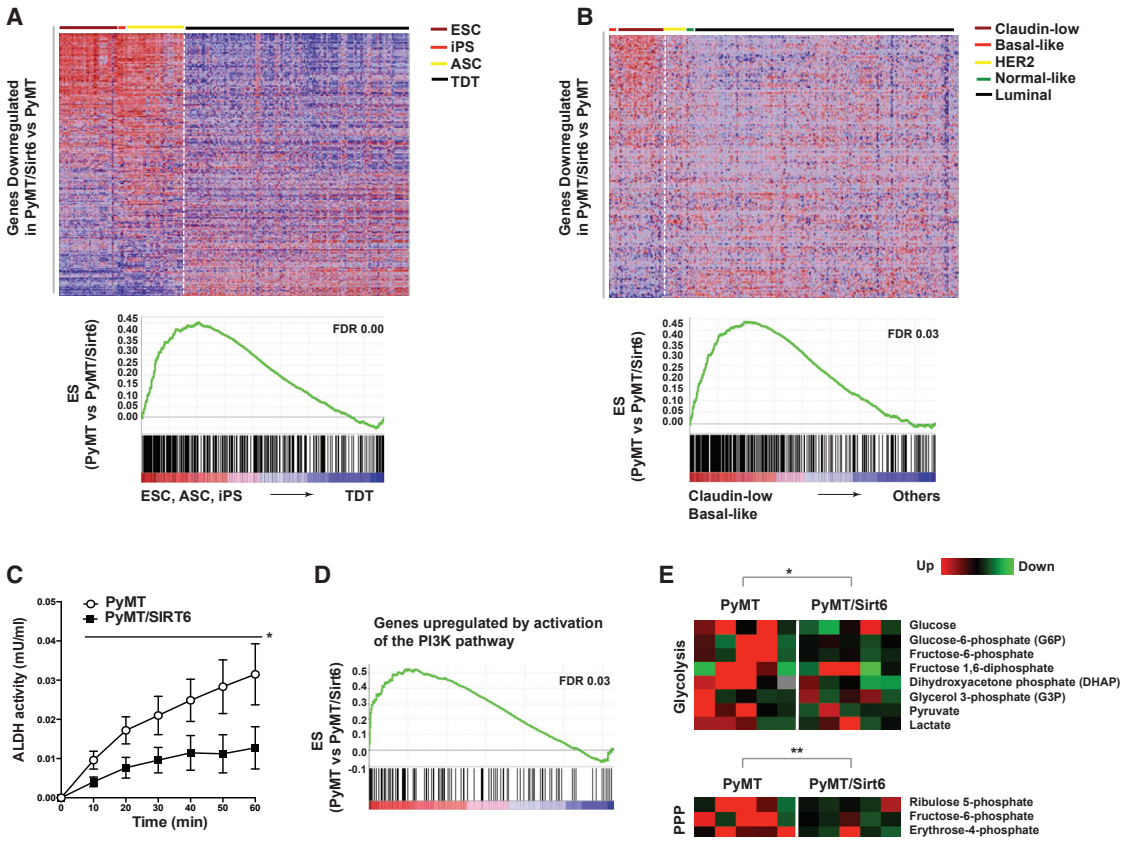

Figure 3. SIRT6 Hinders Stemness of PyMT-Driven Breast Tumors in Mice

(A and B) Enrichment of genes downregulated in PyMT/Sirt6 compared to PyMT tumors were tested in a cohort of public available whole-genome microarrays.

(C) ALDH activity was measured in tumors from 12- to 14-week-old PyMT (n = 6) and PyMT/Sirt6 (n = 6) mice.

(D) Gene set enrichment analysis (GSEA) plot showing the enrichment score (ES) of PI3K's target genes. Gene microarray was performed using RNA extracted from tumors of 12- to 14-week-old PyMT (n = 6) and PyMT/Sirt6 (n = 6) mice.

(E) Pathway enrichment analysis of differentially accumulated metabolites in PyMT/Sirt6 compared to PyMT tumors (n = 6/group). Statistical analysis was done using paired t test between the average values across the samples of each experimental group (PyMT versus PyMT/Sirt6). *$p < 0.05$, **$p < 0.01$.

In (A), (B), and (D), FDR represents false discovery rate q value. In (C), Error bars represent SEM. *$p < 0.05$ (two-tailed unpaired Student's t test). See also Figure S3 and Tables S1 and S2.

test whether SIRT6 overexpression hinder stemness of PyMT-driven breast tumors, we measured ALDH expression and enzymatic activity and found these parameters to be lowered in tumors of PyMT/Sirt6 mice (Figures 3C, S3B, and S3C). We also found that expression of several genes induced by PI3K signaling is downregulated in tumors of PyMT/Sirt6 mice (Figures 3D and S3D). However SIRT6 overexpression did not affect PI3K signaling at the AKT level as the status of AKT phosphorylation was similar in tumors from PyMT/Sirt6 mice and their controls (Figure S2B). These results are in keeping with our in vitro results shown in Figure S1A and suggest that the effect of SIRT6 overexpression on PI3K signaling is downstream of AKT phosphorylation.

Next, we performed a metabolomic assay and found that, while only eight out of 313 biochemicals analyzed display significant changes between groups (Figure S3E; Table S2), pathway analysis indicated that the contents of several intermediate metabolites of glycolysis and the pentose phosphate (PPP) pathways, both of which are boosted by PI3K signaling (Makinoshima et al., 2015; Sun et al., 2011), are lowered in tumors of PyMT/Sirt6 mice compared to controls (Figure 3E). Collectively, our data suggest that enhanced SIRT6 expression exerts anti-tumor action by rearranging metabolism, suppressing PI3K signaling downstream of AKT, and by hindering cancer stem-like attributes of tumors with PI3K activation.

PI3K Activation Is Required for Anti-cancer Stemness Action of SIRT6 Overexpression

To further determine the mechanisms underlying anti-tumor action of SIRT6 overexpression, we focused on PI3K activation as it correlates with responsiveness to SIRT6 overexpression. To directly test whether PI3K activation is required for the anti-tumor action of SIRT6 overexpression, two cell lines derived from DLD-1 cells were transduced with either a control vector or a vector expressing SIRT6. As expected, the latter displayed increased SIRT6 compared to controls (Figure S4A). These genetically modified clones are isogenic except that one bears a wild-type allele (DLD-1-WT), while the other bears the E545K *PIK3CA* allele (DLD-1-MT) (Samuels et al., 2005). In keeping

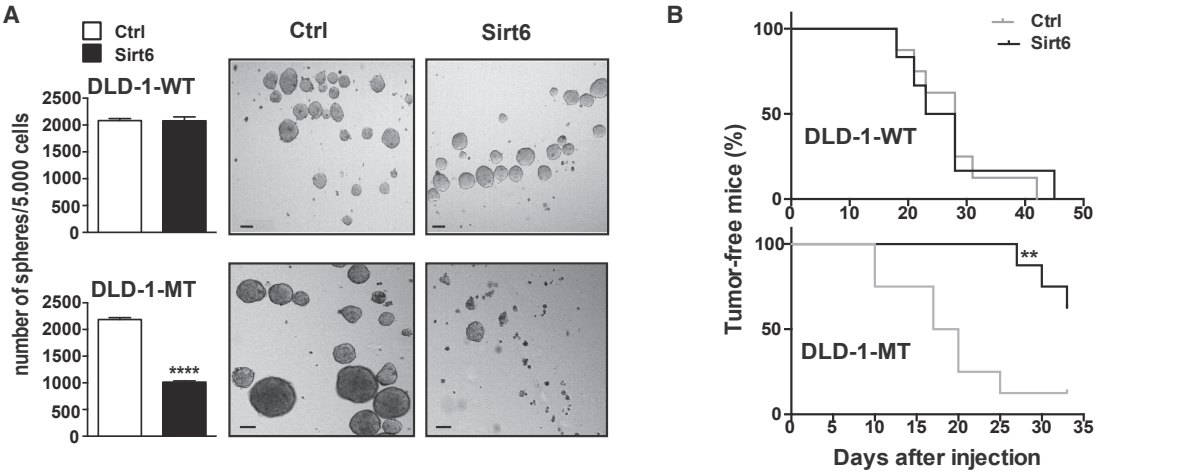

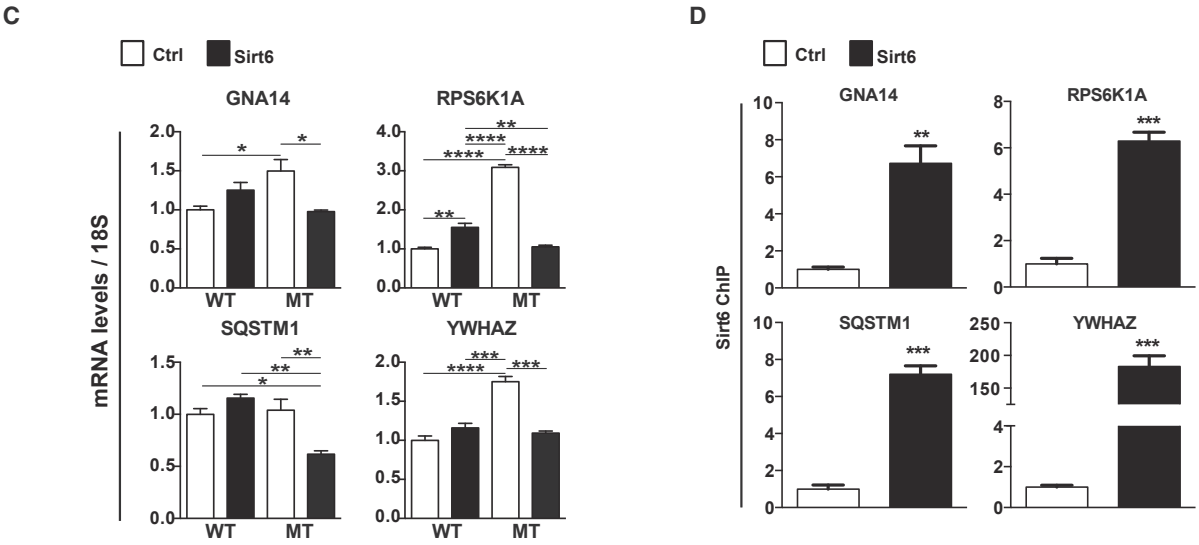

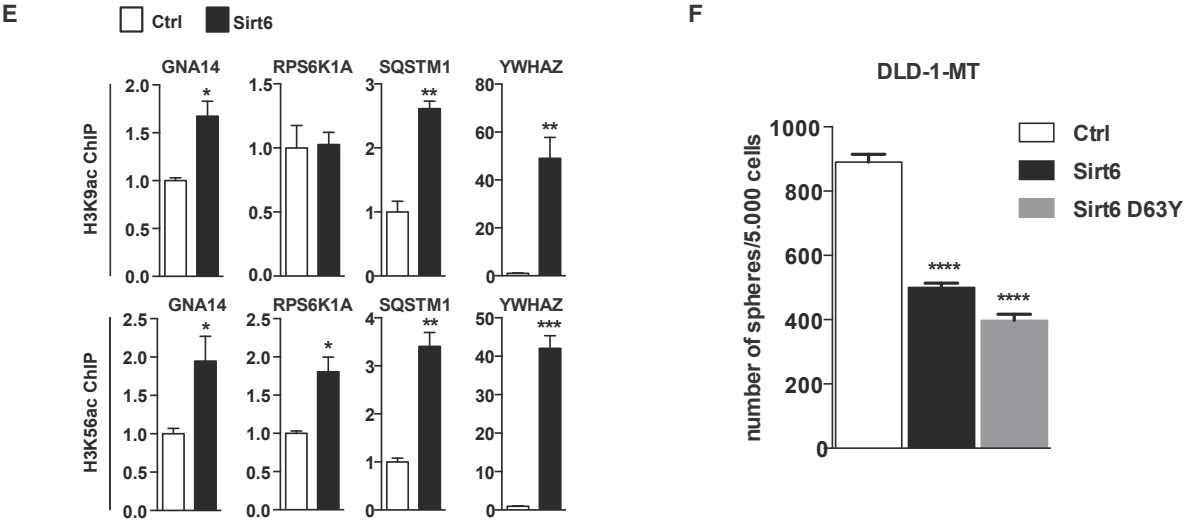

(legend on next page)

with their genetic types, P-S473-AKT/AKT ratio was enhanced in DLD-1-MT compared to DLD-1-WT cells (Figure S4A). In keeping with data shown in Figures S1A and S2A, SIRT6 overexpression did not suppress P-S473-AKT/AKT ratio also in DLD-1-WT and DLD-1-MT cells (Figure S4A). Similar to the effects observed in parental DLD-1 cells, SIRT6 overexpression significantly diminished tumorsphere-forming capacity of DLD-1-MT cells and appearance of DLD-1-MT xenografts (Figures 4A and 4B). However, SIRT6 overexpression was not able to affect these parameters in DLD-1-WT cells and xenografts (Figures 4A and 4B). Together, these results demonstrate that the presence of a PI3K activating mutation is required for the anti-cancer-stemness and -tumor-forming ability of SIRT6 overexpression.

By surveying our transcriptomic and metabolomic data, we noticed that contents of genes and intermediates of the PPP and lipid metabolism (e.g., 1-palmitoylglycerophosphoinositol) pathways were lowered in tumors of PyMT/Sirt6 mice (Figures 3E, S3E, S4B, and S4C). Because PPP is an important source of NADPH for glutathione regeneration and reactive oxygen species (ROS) management, we assessed glutathione and ROS levels in cells with and without SIRT6 overexpression and found no differences between groups (Figures S4D and S4E). Next, we asked whether expression of SIRT6-suppressed lipid metabolism genes is induced by PI3K signaling. Of note, expression of several of these genes was significantly lower in DLD-1-WT compared to DLD-1-MT cells (Figure S4F), hence indicating that removal of the constitutive active PI3K mutation in otherwise isogenic cells suppresses expression of several lipid metabolism genes. Interestingly, a similar effect was observed by SIRT6 overexpression as mRNA content of these lipid metabolism genes was indistinguishable between DLD-1-MT cells overexpressing SIRT6 and DLD-1-WT cells (Figure S4F). Hence, these data suggest that suppression of lipid metabolism genes could be part of the mechanisms by which SIRT6 overexpression dampens CSCs. As many of these genes are implicated in fatty acid oxidation (FAO), we tested the effect of treatment with etomoxir (a clinically tested, specific FAO inhibitor) (Holubarsch et al., 2007). Interestingly, we found that treatment with etomoxir mimics the effect of SIRT6 overexpression as it minimally changed tumorsphere-forming capacity of SIRT6-insensitive cells while strongly reduced tumorsphere-forming capacity of SIRT6-sensitive cells (Figure S4G). Also, combining etomoxir treatment with SIRT6 overexpression had sub-additional effect on tumorsphere-forming capacity of SIRT6-sensitive cells (Figures S4G). Combined with data indicating that SIRT6 overexpression increases ATP content (Figure S4H), our results indicate that FAO inhibition is unlikely to mediate the anti-CSCs action of SIRT6 overexpression; yet, our data suggest that similarly to enhanced SIRT6 action FAO inhibition could be used to dampen stemness of tumors bearing PI3K activation.

Our in vitro and in vivo data shown in Figures S1A, S2A, and S4A strongly indicate that SIRT6 overexpression does not affect AKT phosphorylation; yet, it dampens expression of several PI3K-controlled genes and metabolites (Figures 3D, 3E, S3D, and S4C). Hence, to further explore the mechanism by which SIRT6 suppresses PI3K signaling, we investigated whether SIRT6 overexpression affects the PI3K signaling further downstream of AKT, that is at the transcriptional level. First, we focused on *GNA14*, *RPSK6A1*, *SQSTM1*, and *YWHAZ* because they are known PI3K-controlled genes (Figure S3D). Our data shown in Figure 4C strongly indicate that PI3K signaling induces their expression as *GNA14*, *RPSK6A1*, *SQSTM1*, and *YWHAZ* mRNA level was higher in DLD-1-MT compared to DLD-1-WT cells (Figure 4C). Of note, as it was the case for several PI3K-controlled genes involved in lipid metabolism (Figure S4E), SIRT6 overexpression reduced expression of these genes in DLD-1-MT cells to level similar to DLD-1-WT cells while did not alter (or modestly increased) their expression in DLD-1-WT cells (Figure 4C). Next, we performed chromatin immunoprecipitation (ChIP) for SIRT6 in cancer cells overexpressing SIRT6 and their controls. Our results indicate that indeed SIRT6 binds to promoters of these PI3K-controlled genes and that SIRT6 overexpression increases SIRT6 binding to these promoters (Figure 4D). However, our ChIP assays for acetylated H3K9 and H3K56 (H3K9ac and H3K56ac) indicated that occupancy of H3K9ac and H3K56ac at these promoters was mainly increased (and not decreased as expected) by SIRT6 overexpression (Figure 4E) suggesting that the effect of SIRT6 overexpression on PI3K-controlled genes and potentially on cancer stemness is independent to SIRT6 histone deacetylase activity. To directly test this idea, we overexpressed a deacetylase inactive mutant of SIRT6 bearing a tyrosine instead of an aspartic acid at position 63 (D63Y) (Kugel et al., 2015) in SIRT6-sensitive cells. Because overexpression of SIRT6 or SIRT6 D63Y mutant exerted similar action on tumorsphere-forming capacity of these cells (Figure 4F), we concluded that SIRT6 overexpression suppresses PI3K signaling at the transcriptional level and exerts anti-tumorsphere-forming action via a mechanism independent to its histone deacetylase activity.

DISCUSSION

SIRT6 expression (Kugel et al., 2015; Sebastián et al., 2012; Thirumurthi et al., 2014) and cancer progression and stemness (Pattabiraman et al., 2016; Pattabiraman and Weinberg, 2014; Prost

Figure 4. PI3K Activation Is Required for Anti-cancer Stemness Action of SIRT6 Overexpression

(A) Tumorsphere-forming capacity of indicated cells harboring empty vector (Ctrl) or a vector overexpressing human SIRT6 (Sirt6).

(B) Kaplan-Meier curves comparing percentage of tumor-free mice at different times after subcutaneous injection of indicated cells harboring empty vector (Ctrl) or a vector overexpressing human SIRT6 (Sirt6).

(C) mRNAs levels of PI3K-controlled genes in DLD-1 WT and MT cells harboring empty vector (Ctrl) or a vector overexpressing human SIRT6 (Sirt6).

(D and E) ChIP analysis of SIRT6 (D) and of H3K9ac and H3K56ac (E)on gene promoters in DLD-1 MT cells (in D and E, the data are expressed relative to Ctrl).

(F) Tumorsphere-forming capacity of DLD-1 MT cells harboring empty vector (Ctrl), a vector overexpressing human SIRT6 (Sirt6) or a vector overexpressing a deacetylase inactive mutant of SIRT6 (Sirt6-D63Y). Error bars represent SEM.

In (A), (D), and (E), $^{*}p < 0.05$, $^{**}p < 0.01$, $^{***}p < 0.001$, $^{****}p < 0.0001$ (two-tailed unpaired Student's t test). In (B), $^{**}p < 0.01$, long-rank test. In (C) and (F), $^{*}p < 0.05$, $^{**}p < 0.01$, $^{****}p < 0.0001$ (one-way ANOVA). See also Figure S4.

et al., 2015) are clinically relevant; yet, whether one affects the other is unknown. Here, we provide both in vivo and in vitro evidence that enhanced SIRT6 suppresses cancer progression and stemness. Unexpectedly, this effect is not universal to all cancer types and appears to be independent of the histone deacetylase activity of SIRT6. Indeed, our data indicate that the status of PI3K activation is crucial for determining responsiveness to SIRT6 overexpression. Our transcriptomic and metabolomic results from PyMT-driven breast cancer in mice, as well as both in vitro and in vivo functional assays in human cancer cells with different levels of PI3K signaling, and our ChIP assays strongly indicate that SIRT6 thwarts cancer stemness, at least in part, by suppressing the PI3K pathway at the transcriptional level. While our findings are in keeping with previously published results indicating that SIRT6 negatively regulates PI3K signaling, they indicate that this effect is not dependent on the ability of SIRT6 to deacetylate histone 3 at lysine 9 and/or 56 at promoter regions of PI3K effector genes as previously suggested (Sundaresan et al., 2012). A deacetylase-independent action is not at odds with the fact that others have shown very minor histone deacetylase ability of SIRT6 (Jiang et al., 2013; Liszt et al., 2005). As activation of PI3K signaling promotes survival of CSCs (Hambardzumyan et al., 2008; Jiang et al., 2015), our data support a model whereby enhanced SIRT6 dampens PI3K signaling at the transcriptional level, an effect that leads to several changes, including altered glucose and lipid metabolism and reduced cancer stemness. Because SIRT6 overexpression dampens expression of a large number of genes, we suggest that its anti-cancer-stemness action is brought about by a concerted rather than a single mechanistic change. It is important to keep in mind that in addition to PI3K activation our results do not exclude the possibility that SIRT6 overexpression may influence behavior of tumors bearing other types of mutations. Hence, further analysis aimed at testing the effect of SIRT6 overexpression in a large panel of tumors bearing a wide range of different mutations is warranted.

Augmented SIRT6 function has been shown to bring about beneficial effects in the context of metabolism (Anderson et al., 2015) and aging (Kanfi et al., 2012); thus, combined with results reported herein these data provide rationale for developing SIRT6 agonists as therapeutics for age-related diseases (e.g., cancer and diabetes). Furthermore, our findings are relevant in a personalized medicine context as they could be used to stratify patients bearing tumors with PI3K activation into likely responders to means aimed at increasing SIRT6 function.

EXPERIMENTAL PROCEDURES

Mouse Generation and Studies

MMTV-PyMT mice were generated as previously described (Guy et al., 1992). Sirt6BAC mice were generated by BAC transgenesis as described previously (Anderson et al., 2015) and are available from The Jackson Laboratory (JAX#028361). Mice were housed in groups of four or five with food and water available ad libitum in light- and temperature-controlled environments. Care of mice was within the procedures approved by animal care and experimentation authorities of the Canton of Geneva, Switzerland.

SIRT6 Overexpression in Cancer Cells

We produced recombinant retroviruses by transfecting Phoenix-Ampho cells (ATCC), using TransIT-293 transfection reagent (Mirus) and pBABE retroviral constructs. Cells were transfected with pBABE vectors expressing human-SIRT6, or deacetylase-dead human-SIRT6 bearing a tyrosine instead of an aspartic acid at position 63 (D63Y) (Kugel et al., 2015), or pBABE empty vector and selected for puromycin resistance.

In Vitro Assessment of Cell Proliferation

Cells were fixed with formalin and stained with Crystal Violet (CV). Then, CV-stained cells were dissolved with 5% acetic acid for 30 min and 200 μL of this solution was transferred to a 96-well plate and read in a plate reader at 570 nm. T1 and T2 values were normalized to T0. Proliferation curves were compared between groups and experiments were repeated at least three times.

Tumorsphere Assays

Tumorsphere formation was induced in ultralow-adherent 6-well plates. Cells were plated at a density of 5,000 cells per well in triplicate in a 6-well plate in a 1% methylcellulose containing media (MammoCult supplemented with MethoCult media, STEMCELL Technologies). Tumorsphere formation was quantified 7 days after plating. Spheres with a diameter equal or higher than 50 μm were deemed tumorspheres. Etomoxir (Sigma) was added at the specified concentrations to the media. Experiments were repeated at least three times.

Mouse Xenograft Assay

Cells were trypsinized, suspended in PBS, and injected subcutaneously into the flank of NOD/SCID mice. Cells were injected at the following numbers: 1×10^6 and 1×10^4 MCF10DCIS, 1×10^6 MDA-MB-231, 1×10^5 H1650, 1×10^5 DLD-1 MT, and 1×10^5 DLD-1 WT cells. Mice were checked twice a week for tumor appearance and tumor diameter measurements.

Tumor Grade Assessment

Mice bearing at least one tumor with 10 mm of major diameter (as measured manually with a caliper) were sacrificed and all their detectable tumors collected. Tumors of comparable size were used for histologic analysis. Areas of different histological types (adenoma, hyperplasia, necrosis, and carcinoma) were assessed by surveying the whole tumor area as previously described (Santidrian et al., 2013).

mRNA and Protein Contents

Mice were sacrificed, and tissues were quickly removed and snap-frozen in liquid nitrogen and subsequently stored at – 80°C. RNAs were extracted using TRIzol reagent (Invitrogen). Complementary DNA was generated by Superscript II (Invitrogen) and used with SYBR Green PCR master mix (Applied Biosystems) for real-time qPCR analysis. mRNA contents were normalized to *β-actin* and/or *36B4* mRNA levels. All assays were performed using an Applied Biosystems QuantStudio 5 Real-Time PCR System. For each mRNA assessment, real-time qPCR analyses were repeated at least three times. Proteins were extracted by homogenizing samples in lysis buffer (Tris 20 mM, EDTA 5 mM, NP40 1% [v/v], protease inhibitors [P2714-1BTL from Sigma]) and then resolved by SDS-PAGE and finally transferred to a nitrocellulose membrane by electroblotting. Proteins were detected using commercially available antisera as previously described (Ramadori et al., 2011, 2015).

ALDH Activity

ALDH activity was assessed using the ALDH Activity Colorimetric Assay Kit from Biovision (K731-100) and following the manufacturer's instructions. Briefly, samples were homogenized with 200 μL of ice-cold ALDH assay buffer, and 3 μL of the homogenate was used in the assay. Absorbance was measured at 450 nm every 5 min over 1 hr, and the oxidation of Acetaldehyde to NADH was calculated according to the manufacturer's instructions.

FACS

ALDH activity was measured in cancer cells using the Aldefluor kit following the manufacturer protocol. 5×10^5 of H1650 or MCF10DCIS cells were incubated with Aldefluor reagent and N,N-diethylaminobenzaldehyde (DEAB; represented in blue) or Aldefluor reagent only (represented in red). After a 40-min incubation period, cells were analyzed by flow cytometry, and results were generated using FlowJo software. Values mentioned along with the graphs indicate percentage of cells with high ALDH activity.

Microarray and Metabolomic Assays

Mice were sacrificed, and tissues were quickly removed, frozen in liquid nitrogen, and subsequently stored at –80°C. RNAs were extracted by QIAGEN mRNA extract kits (RNeasy plus). Microarray analyses were performed by University of Texas Southwestern Medical Center at Dallas microarray Core facility (https://microarray.swmed.edu/) using Illumina Chip Mouse WG-6 v.2.0 (Illumina). Metabolites contents were measured by Metabolon. The differential analysis of the transcriptomic and metabolomic data were performed using CyberT (Baldi and Long, 2001; Kayala and Baldi, 2012). Briefly, the average signal intensity was transformed using a log base 2 normalization, and a regularized t test was then performed using Cyber-T with a window size of 51 and a Bayesian confidence value of 5. p values of 0.001 and 0.01 were considered significant for microarray and metabolomics analyses, respectively. Pathway and functional enrichment was carried out using DAVID (Huang et al., 2009).

Chromatin Immunoprecipitation Assays

ChIP assays were performed as previously described (Kugel et al., 2016; Sebastián et al., 2012). Antibodies used are 5 μL anti-SIRT6 (Abcam; ab62739), 5 μL anti-H3K9Ac (Millipore 07-352), and 5 μL anti-H3K56Ac (ab76307). Data were normalized to values obtained with unspecific immunoglobulin Gs (IgGs) (Abcam).

Determination of the Cellular Glutathione Content

Cells were seeded in 96-well plate at a density of 10^4 per well and incubated (protected from the light) with 20 μM monobromobimane (mBBr) for 10 min at 37°C. The conjugation of glutathione with monobromobimane was followed by measuring the fluorescent product at Ex/Em 394/490 nm using SpectraMax Paradigm microplate reader (Molecular Devices). The results are expressed as a percentage of the glutathione content in control cells.

Determination of Mitochondrial ROS Content

5×10^4 cells in Hank's balanced salt solution (HBSS), 10 mM HEPES (pH 7.4), 17.5 mM glucose, 1.55 mM $CaCl_2$, and 10% FBS were incubated with 5 μM MitoSox (Thermo Fisher Scientific) for exactly 10 min at room temperature before analysis on a CyAn flow cytometer (Beckman Coulter).

ATP Determination in Tumorspheres

Cells were lysed with 10% trichloroacetic acid × 30 min in ice. Next, the lysate was centrifuged at 13,000 rpm for 5 min at 4 degrees and a 1/16 dilution of the supernatant (in distillated ultrapure water) was used for ATP determination using a commercial kit (Molecular Probe #A22066) according to the manufacturer's instructions. Values were normalized to lysate protein contents.

Dataset Compilation

Datasets of stem cells (ESCs, ASCs, and iPS cells) and terminally differentiated tissues (TDTs) was generated by compiling 246 whole-genome microarray datasets downloaded form ArrayExpress database (https://www.ebi.ac.uk/arrayexpress/). In order to avoid inter-platform biases, only data generated using the same microarray platform (Affimetrix 430 2.0) were selected. Microarrays were downloaded as raw files, concatenated in a unique dataset and normalized according to the Robust Multichip Average (RMA) algorithm.

Statistical Analyses

Data are reported as mean ± SEM. Statistical analyses were performed using GraphPad Prism 6.0c software. Unpaired two-tailed t tests were employed when two groups were compared, and one-way ANOVA with Tukey correction for multiple comparisons was used when three or more groups were compared unless otherwise specified.

ACCESSION NUMBERS

The accession number for the microarray data from tumor tissues of PyMT and PyMT/Sirt6 mice reported in this paper is NCBI Gene Expression Omnibus: GSE93837.

SUPPLEMENTAL INFORMATION

Supplemental Information includes four figures and two tables and can be found with this article online at http://dx.doi.org/10.1016/j.celrep.2017.01.065.

AUTHOR CONTRIBUTIONS

Conceptualization, R.C., M.G., R.M.I., and G.R.; Investigation, M.G., R.M.I., G.R., J.G.A., A.C., G.K., X.B., E.A., A.G., C.S., R.M., D.M., and N.C.; Writing – Original Draft, R.C.; Writing – Review & Editing, R.C., M.G., R.M.I., G.R., and P.B.; Funding Acquisition, R.M.I., R.C., and P.B.; Data Curation, R.C., M.G., R.M.I., P.B., N.C., and G.R.; Supervision, R.C. and G.R.

ACKNOWLEDGMENTS

We thank Carolyn Heckenmeyer and Ariane Widmer in the Coppari laboratory for their technical support, Drs. Claes Wollheim, Mirko Trajkovski, PierPaolo Scaglioni, and Nima Sharifi for suggestions and critical reading of the manuscript, and Dr. Philipp E. Scherer for providing MMTV-PyMT mice. This work was supported in part by Coordenação de Aperfeiçoamento de Pessoal de Nível Superior (CAPES graduate student fellowship to R.M.I.), European Commission (Marie Curie Career Integration grant 320898 and ERC-Consolidator grant 614847), the Swiss National Science Foundation (310030_146533/1), the Swiss Cancer League (KLS-3794-02-2016-R), the Louis-Jeantet Foundation, the Gertrude von Meissner Foundation, and the Fondation Pour Recherches Medicales of the University of Geneva to R.C. The work of N.C. and P.B. was in part supported by NIH grant LM 010235 to P.B.

Received: June 16, 2016
Revised: December 22, 2016
Accepted: January 25, 2017
Published: February 21, 2017

REFERENCES

Anderson, J.G., Ramadori, G., Ioris, R.M., Galiè, M., Berglund, E.D., Coate, K.C., Fujikawa, T., Pucciarelli, S., Moreschini, B., Amici, A., et al. (2015). Enhanced insulin sensitivity in skeletal muscle and liver by physiological overexpression of SIRT6. Mol. Metab. *4*, 846–856.

Baldi, P., and Long, A.D. (2001). A Bayesian framework for the analysis of microarray expression data: Regularized t -test and statistical inferences of gene changes. Bioinformatics *17*, 509–519.

Barger, J.L., Kayo, T., Vann, J.M., Arias, E.B., Wang, J., Hacker, T.A., Wang, Y., Raederstorff, D., Morrow, J.D., Leeuwenburgh, C., et al. (2008). A low dose of dietary resveratrol partially mimics caloric restriction and retards aging parameters in mice. PLoS ONE *3*, e2264.

Ben-Porath, I., Thomson, M.W., Carey, V.J., Ge, R., Bell, G.W., Regev, A., and Weinberg, R.A. (2008). An embryonic stem cell-like gene expression signature in poorly differentiated aggressive human tumors. Nat. Genet. *40*, 499–507.

Carpentino, J.E., Hynes, M.J., Appelman, H.D., Zheng, T., Steindler, D.A., Scott, E.W., and Huang, E.H. (2009). Aldehyde dehydrogenase-expressing colon stem cells contribute to tumorigenesis in the transition from colitis to cancer. Cancer Res. *69*, 8208–8215.

Cheung, A.M., Wan, T.S., Leung, J.C., Chan, L.Y., Huang, H., Kwong, Y.L., Liang, R., and Leung, A.Y. (2007). Aldehyde dehydrogenase activity in leukemic blasts defines a subgroup of acute myeloid leukemia with adverse prognosis and superior NOD/SCID engrafting potential. Leukemia *21*, 1423–1430.

Dontu, G., Abdallah, W.M., Foley, J.M., Jackson, K.W., Clarke, M.F., Kawamura, M.J., and Wicha, M.S. (2003). In vitro propagation and transcriptional profiling of human mammary stem/progenitor cells. Genes Dev. *17*, 1253–1270.

Ginestier, C., Hur, M.H., Charafe-Jauffret, E., Monville, F., Dutcher, J., Brown, M., Jacquemier, J., Viens, P., Kleer, C.G., Liu, S., et al. (2007). ALDH1 is a marker of normal and malignant human mammary stem cells and a predictor of poor clinical outcome. Cell Stem Cell *1*, 555–567.

Guy, C.T., Cardiff, R.D., and Muller, W.J. (1992). Induction of mammary tumors by expression of polyomavirus middle T oncogene: A transgenic mouse model for metastatic disease. Mol. Cell. Biol. *12*, 954–961.

Hambardzumyan, D., Becher, O.J., Rosenblum, M.K., Pandolfi, P.P., Manova-Todorova, K., and Holland, E.C. (2008). PI3K pathway regulates survival of cancer stem cells residing in the perivascular niche following radiation in medulloblastoma in vivo. Genes Dev. *22*, 436–448.

Holubarsch, C.J., Rohrbach, M., Karrasch, M., Boehm, E., Polonski, L., Ponikowski, P., and Rhein, S. (2007). A double-blind randomized multicentre clinical trial to evaluate the efficacy and safety of two doses of etomoxir in comparison with placebo in patients with moderate congestive heart failure: The ERGO (etomoxir for the recovery of glucose oxidation) study. Clin. Sci. *113*, 205–212.

Huang, W., Sherman, B.T., and Lempicki, R.A. (2009). Bioinformatics enrichment tools: Paths toward the comprehensive functional analysis of large gene lists. Nucleic Acids Res. *37*, 1–13.

Jiang, H., Khan, S., Wang, Y., Charron, G., He, B., Sebastian, C., Du, J., Kim, R., Ge, E., Mostoslavsky, R., et al. (2013). SIRT6 regulates TNF-α secretion through hydrolysis of long-chain fatty acyl lysine. Nature *496*, 110–113.

Jiang, A.G., Lu, H.Y., Zhang, D.G., Zhang, L.X., and Gao, X.Y. (2015). Short hairpin RNA targeting AKT1 and PI3K/p85 suppresses the proliferation and self-renewal of lung cancer stem cells. Mol. Med. Rep. *12*, 363–370.

Kalaany, N.Y., and Sabatini, D.M. (2009). Tumours with PI3K activation are resistant to dietary restriction. Nature *458*, 725–731.

Kanfi, Y., Naiman, S., Amir, G., Peshti, V., Zinman, G., Nahum, L., Bar-Joseph, Z., and Cohen, H.Y. (2012). The sirtuin SIRT6 regulates lifespan in male mice. Nature *483*, 218–221.

Kawahara, T.L., Rapicavoli, N.A., Wu, A.R., Qu, K., Quake, S.R., and Chang, H.Y. (2011). Dynamic chromatin localization of Sirt6 shapes stress- and aging-related transcriptional networks. PLoS Genet. *7*, e1002153.

Kayala, M.A., and Baldi, P. (2012). Cyber-T web server: Differential analysis of high-throughput data. Nucleic Acids Res. *40*, W553–W559.

Kugel, S., Feldman, J.L., Klein, M.A., Silberman, D.M., Sebastián, C., Mermel, C., Dobersch, S., Clark, A.R., Getz, G., Denu, J.M., and Mostoslavsky, R. (2015). Identification of and molecular basis for SIRT6 loss-of-function point mutations in cancer. Cell Rep. *13*, 479–488.

Kugel, S., Sebastián, C., Fitamant, J., Ross, K.N., Saha, S.K., Jain, E., Gladden, A., Arora, K.S., Kato, Y., Rivera, M.N., et al. (2016). SIRT6 suppresses pancreatic cancer through control of Lin28b. Cell *165*, 1401–1415.

Lapidot, T., Sirard, C., Vormoor, J., Murdoch, B., Hoang, T., Caceres-Cortes, J., Minden, M., Paterson, B., Caligiuri, M.A., and Dick, J.E. (1994). A cell initiating human acute myeloid leukaemia after transplantation into SCID mice. Nature *367*, 645–648.

Lin, E.Y., Jones, J.G., Li, P., Zhu, L., Whitney, K.D., Muller, W.J., and Pollard, J.W. (2003). Progression to malignancy in the polyoma middle T oncoprotein mouse breast cancer model provides a reliable model for human diseases. Am. J. Pathol. *163*, 2113–2126.

Liszt, G., Ford, E., Kurtev, M., and Guarente, L. (2005). Mouse Sir2 homolog SIRT6 is a nuclear ADP-ribosyltransferase. J. Biol. Chem. *280*, 21313–21320.

Liu, S., Ginestier, C., Ou, S.J., Clouthier, S.G., Patel, S.H., Monville, F., Korkaya, H., Heath, A., Dutcher, J., Kleer, C.G., et al. (2011). Breast cancer stem cells are regulated by mesenchymal stem cells through cytokine networks. Cancer Res. *71*, 614–624.

Makinoshima, H., Takita, M., Saruwatari, K., Umemura, S., Obata, Y., Ishii, G., Matsumoto, S., Sugiyama, E., Ochiai, A., Abe, R., et al. (2015). Signaling through the phosphatidylinositol 3-kinase (PI3K)/mammalian target of rapamycin (mTOR) axis is responsible for aerobic glycolysis mediated by glucose transporter in epidermal growth factor receptor (EGFR)-mutated lung adenocarcinoma. J. Biol. Chem. *290*, 17495–17504.

Mikkelsen, T.S., Ku, M., Jaffe, D.B., Issac, B., Lieberman, E., Giannoukos, G., Alvarez, P., Brockman, W., Kim, T.K., Koche, R.P., et al. (2007). Genome-wide maps of chromatin state in pluripotent and lineage-committed cells. Nature *448*, 553–560.

Mikkelsen, T.S., Hanna, J., Zhang, X., Ku, M., Wernig, M., Schorderet, P., Bernstein, B.E., Jaenisch, R., Lander, E.S., and Meissner, A. (2008). Dissecting direct reprogramming through integrative genomic analysis. Nature *454*, 49–55.

Ming, M., Han, W., Zhao, B., Sundaresan, N.R., Deng, C.X., Gupta, M.P., and He, Y.Y. (2014). SIRT6 promotes COX-2 expression and acts as an oncogene in skin cancer. Cancer Res. *74*, 5925–5933.

Pattabiraman, D.R., and Weinberg, R.A. (2014). Tackling the cancer stem cells - what challenges do they pose? Nat. Rev. Drug Discov. *13*, 497–512.

Pattabiraman, D.R., Bierie, B., Kober, K.I., Thiru, P., Krall, J.A., Zill, C., Reinhardt, F., Tam, W.L., and Weinberg, R.A. (2016). Activation of PKA leads to mesenchymal-to-epithelial transition and loss of tumor-initiating ability. Science *351*, aad3680.

Ponti, D., Costa, A., Zaffaroni, N., Pratesi, G., Petrangolini, G., Coradini, D., Pilotti, S., Pierotti, M.A., and Daidone, M.G. (2005). Isolation and in vitro propagation of tumorigenic breast cancer cells with stem/progenitor cell properties. Cancer Res. *65*, 5506–5511.

Prost, S., Relouzat, F., Spentchian, M., Ouzegdouh, Y., Saliba, J., Massonnet, G., Beressi, J.P., Verhoeyen, E., Raggueneau, V., Maneglier, B., et al. (2015). Erosion of the chronic myeloid leukaemia stem cell pool by PPARγ agonists. Nature *525*, 380–383.

Ramadori, G., Fujikawa, T., Anderson, J., Berglund, E.D., Frazao, R., Michán, S., Vianna, C.R., Sinclair, D.A., Elias, C.F., and Coppari, R. (2011). SIRT1 deacetylase in SF1 neurons protects against metabolic imbalance. Cell Metab. *14*, 301–312.

Ramadori, G., Konstantinidou, G., Venkateswaran, N., Biscotti, T., Morlock, L., Galié, M., Williams, N.S., Luchetti, M., Santinelli, A., Scaglioni, P.P., and Coppari, R. (2015). Diet-induced unresolved ER stress hinders KRAS-driven lung tumorigenesis. Cell Metab. *21*, 117–125.

Rasheed, Z.A., Yang, J., Wang, Q., Kowalski, J., Freed, I., Murter, C., Hong, S.M., Koorstra, J.B., Rajeshkumar, N.V., He, X., et al. (2010). Prognostic significance of tumorigenic cells with mesenchymal features in pancreatic adenocarcinoma. J. Natl. Cancer Inst. *102*, 340–351.

Sampath, P., Pritchard, D.K., Pabon, L., Reinecke, H., Schwartz, S.M., Morris, D.R., and Murry, C.E. (2008). A hierarchical network controls protein translation during murine embryonic stem cell self-renewal and differentiation. Cell Stem Cell *2*, 448–460.

Samuels, Y., Diaz, L.A., Jr., Schmidt-Kittler, O., Cummins, J.M., Delong, L., Cheong, I., Rago, C., Huso, D.L., Lengauer, C., Kinzler, K.W., et al. (2005). Mutant PIK3CA promotes cell growth and invasion of human cancer cells. Cancer Cell *7*, 561–573.

Santidrian, A.F., Matsuno-Yagi, A., Ritland, M., Seo, B.B., LeBoeuf, S.E., Gay, L.J., Yagi, T., and Felding-Habermann, B. (2013). Mitochondrial complex I activity and NAD+/NADH balance regulate breast cancer progression. J. Clin. Invest. *123*, 1068–1081.

Seale, P., Kajimura, S., Yang, W., Chin, S., Rohas, L.M., Uldry, M., Tavernier, G., Langin, D., and Spiegelman, B.M. (2007). Transcriptional control of brown fat determination by PRDM16. Cell Metab. *6*, 38–54.

Sebastián, C., Zwaans, B.M., Silberman, D.M., Gymrek, M., Goren, A., Zhong, L., Ram, O., Truelove, J., Guimaraes, A.R., Toiber, D., et al. (2012). The histone deacetylase SIRT6 is a tumor suppressor that controls cancer metabolism. Cell *151*, 1185–1199.

Sorlie, T., Tibshirani, R., Parker, J., Hastie, T., Marron, J.S., Nobel, A., Deng, S., Johnsen, H., Pesich, R., Geisler, S., et al. (2003). Repeated observation of breast tumor subtypes in independent gene expression data sets. Proc. Natl. Acad. Sci. USA *100*, 8418–8423.

Sos, M.L., Koker, M., Weir, B.A., Heynck, S., Rabinovsky, R., Zander, T., Seeger, J.M., Weiss, J., Fischer, F., Frommolt, P., et al. (2009). PTEN loss contributes to erlotinib resistance in EGFR-mutant lung cancer by activation of Akt and EGFR. Cancer Res. *69*, 3256–3261.

Su, Y., Subedee, A., Bloushtain-Qimron, N., Savova, V., Krzystanek, M., Li, L., Marusyk, A., Tabassum, D.P., Zak, A., Flacker, M.J., et al. (2015). Somatic Cell

Fusions Reveal Extensive Heterogeneity in Basal-like Breast Cancer. Cell Rep. *11*, 1549–1563.

Subramanian, A., Tamayo, P., Mootha, V.K., Mukherjee, S., Ebert, B.L., Gillette, M.A., Paulovich, A., Pomeroy, S.L., Golub, T.R., Lander, E.S., and Mesirov, J.P. (2005). Gene set enrichment analysis: A knowledge-based approach for interpreting genome-wide expression profiles. Proc. Natl. Acad. Sci. USA *102*, 15545–15550.

Sun, Q., Chen, X., Ma, J., Peng, H., Wang, F., Zha, X., Wang, Y., Jing, Y., Yang, H., Chen, R., et al. (2011). Mammalian target of rapamycin up-regulation of pyruvate kinase isoenzyme type M2 is critical for aerobic glycolysis and tumor growth. Proc. Natl. Acad. Sci. USA *108*, 4129–4134.

Sundaresan, N.R., Vasudevan, P., Zhong, L., Kim, G., Samant, S., Parekh, V., Pillai, V.B., Ravindra, P.V., Gupta, M., Jeevanandam, V., et al. (2012). The sirtuin SIRT6 blocks IGF-Akt signaling and development of cardiac hypertrophy by targeting c-Jun. Nat. Med. *18*, 1643–1650.

Thirumurthi, U., Shen, J., Xia, W., LaBaff, A.M., Wei, Y., Li, C.W., Chang, W.C., Chen, C.H., Lin, H.K., Yu, D., and Hung, M.C. (2014). MDM2-mediated degradation of SIRT6 phosphorylated by AKT1 promotes tumorigenesis and trastuzumab resistance in breast cancer. Sci. Signal. *7*, ra71.

Thorrez, L., Van Deun, K., Tranchevent, L.C., Van Lommel, L., Engelen, K., Marchal, K., Moreau, Y., Van Mechelen, I., and Schuit, F. (2008). Using ribosomal protein genes as reference: A tale of caution. PLoS ONE *3*, e1854.

Ulloa-Montoya, F., Kidder, B.L., Pauwelyn, K.A., Chase, L.G., Luttun, A., Crabbe, A., Geraerts, M., Sharov, A.A., Piao, Y., Ko, M.S., et al. (2007). Comparative transcriptome analysis of embryonic and adult stem cells with extended and limited differentiation capacity. Genome Biol. *8*, R163.

van de Vijver, M.J., He, Y.D., van't Veer, L.J., Dai, H., Hart, A.A., Voskuil, D.W., Schreiber, G.J., Peterse, J.L., Roberts, C., Marton, M.J., et al. (2002). A gene-expression signature as a predictor of survival in breast cancer. N. Engl. J. Med. *347*, 1999–2009.

Van Meter, M., Mao, Z., Gorbunova, V., and Seluanov, A. (2011). SIRT6 overexpression induces massive apoptosis in cancer cells but not in normal cells. Cell Cycle *10*, 3153–3158.

Wang, J.C., and Dick, J.E. (2005). Cancer stem cells: Lessons from leukemia. Trends Cell Biol. *15*, 494–501.

Yang, X., Lin, X., Zhong, X., Kaur, S., Li, N., Liang, S., Lassus, H., Wang, L., Katsaros, D., Montone, K., et al. (2010). Double-negative feedback loop between reprogramming factor LIN28 and microRNA let-7 regulates aldehyde dehydrogenase 1-positive cancer stem cells. Cancer Res. *70*, 9463–9472.